Journal of Merchant Ship Wind Energy

Wind tunnel tests for a six-masted sailing vessel by Prölss: Translation of B. Wagner's "Windkanalversuche für einen sechsmastigen Segler nach Prölss"

Lubomir A. Ribarov, Ph.D., Department of Marine Engineering, U.S. Merchant Marine Academy, Kings Point, NY, September 2022 ribarovl@usmma.edu

Originally published in German by Institute for Shipbuilding of the University of Hamburg, Report No. 173, 1967, Windkanalversuche für einen sechsmastigen Segler nach Prölss".

ABSTRACT

Tests were carried out in the IfS wind tunnel on a model of a new sailing ship, and the results described. The rigging of the new sailing vessel corresponds to a design by W. Prölss. The results are presented in dimensionless form, namely the horizontal force components and the yaw and roll moments, as a function of mast setting and lateral wind angle. The sailing polars were compared to sail polars of a conventional four-masted barque. The comparison shows the propulsion forces of sailing ships is greatly improved by the use of modern sail designs.

1. Introduction

Wind tunnel tests with the rigging model of a four-masted barque are described in Report No. 172 of the Institute for Shipbuilding [2]. This current publication, which is an abbreviated version of IfS[1] Report No. 173 [1] in both text- and images, contains wind tunnel test results of a model of a six-masted sailing vessel by Prölss[2]. This investigation, as part of a larger research project "Wind Forces on Ships", funded by the Research Council of the Free and Hanseatic City of Hamburg, compares sail forces of modern, newly designed sailing ships with traditional sailing vessels. With the help of a method developed at the IfS [3], the speed of modern and conventional sailing vessels may be calculated, permitting an analysis of the commercial viability of these vessels.

Here a sailing vessel with square-rigged masts by W. Prölss is considered. The construction consists of curved yards on a cantilever elliptical profile mast, whereby the entire mast being set between yards and sails forms a closed arched and relatively stable surface shape. The basic aerodynamic characteristics of the Prölss rig can be determined by measurements of the panel sails. Such panel sails measurements have been performed on single masts as well as on panel sails in multi-masted arrangement [4], [5], [6]. The result of these preliminary investigations can be summarized as follows:

1. The individual masts should - when compared with more pronounced curvatures - be more favorable in the case of multi-mast arrangements for propulsion effect in forward to lateral winds where a circular curvature (camber) of the yards from $f/L_S = 0.120$ is used.

2. Using a six-masted ship with masts closer together than optimal, results in a degradation of the drag polar, but not so large that a five-masted ship with optimal spacing is better, assuming the same sail area.

3. The sail polar plots of a multi-masted vessel can be significantly improved by increasing the setting angle into the wind, as one moves aft.

2. Test Facility and Model

2.1. Test Facility

The tests took place in the IfS wind tunnel. The model was placed on a square base plate of 1.75 m x 1.05 m (limiting the beam below) embedded on a rotating turntable. The test facility was described and explained through a sketch (drawing) in an IfS report No. 172 [2]. The electric three-component scale, connected to the turntable, allows the measurement of resistance (force component in flow direction), lateral force (force component perpendicular to the flow direction), and yaw moment.

---

[1] IfS = Institut für Schiffbau (Institute for Shipbuilding) – where B. Wagner worked at the TUHH (translator's remark)

[2] Wilhelm Prölss (1901 – 1974) was a shipbuilding engineer who, in the early 1960s, developed the yards-based sail system called Dyna-Rigg , which was originally intended for making cargo sail ships more cost-effective. https://de.wikipedia.org/wiki/Dyna-Rigg (translator's remark)

In addition, a rolling moments scale was placed in the turntable. For this purpose, a second plate was created with the adjustable floor of the model tub[3] connected with two steel springs, on which DMS[4] strips are attached. The model was screwed on to the second plate. Elastic foam strips were used to seal the model tub at the waterline of the stencils covered model. The rolling moment scale was calibrated with the built-in waterline sealed model so that the elastic properties of the seal are taken into account.

2.2. Model

The wind tunnel model is based on a design draft by Ingenieurkontor Lübeck (IKL)[5] for a six-masted bulk carrier sailing ship by Prölss. The structures were, to some extent, greatly simplified. In addition, the measurement was only for construction (design) draft. This is sufficient given the hull forces are small compared to the forces on the sails. Please see Figures 1-3.

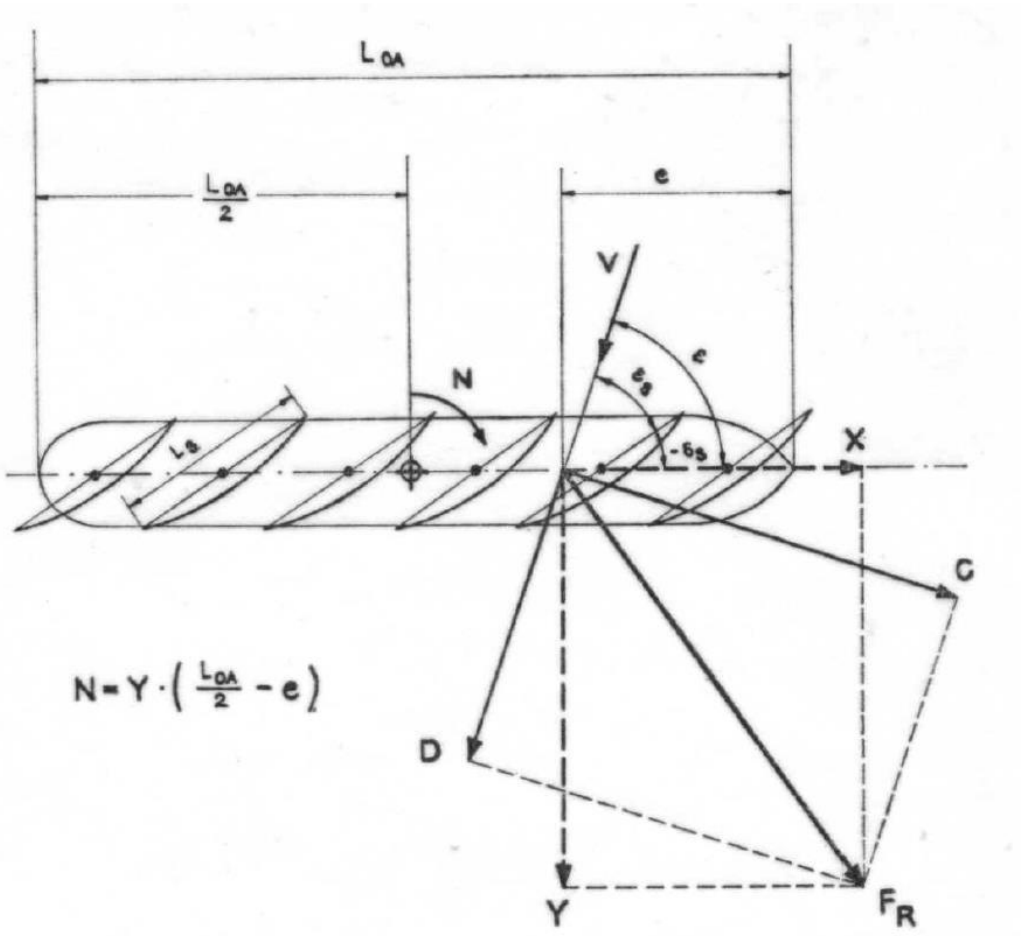

Figure 1. Important Parameters used in this report.

[3] Although the direct translation of "Wanne" is "tub," it seems that a better English word may be "trough" (translator's remark)
[4] DMS = Datenmesssystem – Data measurement system (translator's remark)
[5] Ingenieurkontor Lübeck (IKL) GmbH – a naval architecture and design firm located in Kiel, Germany (translator's remark)

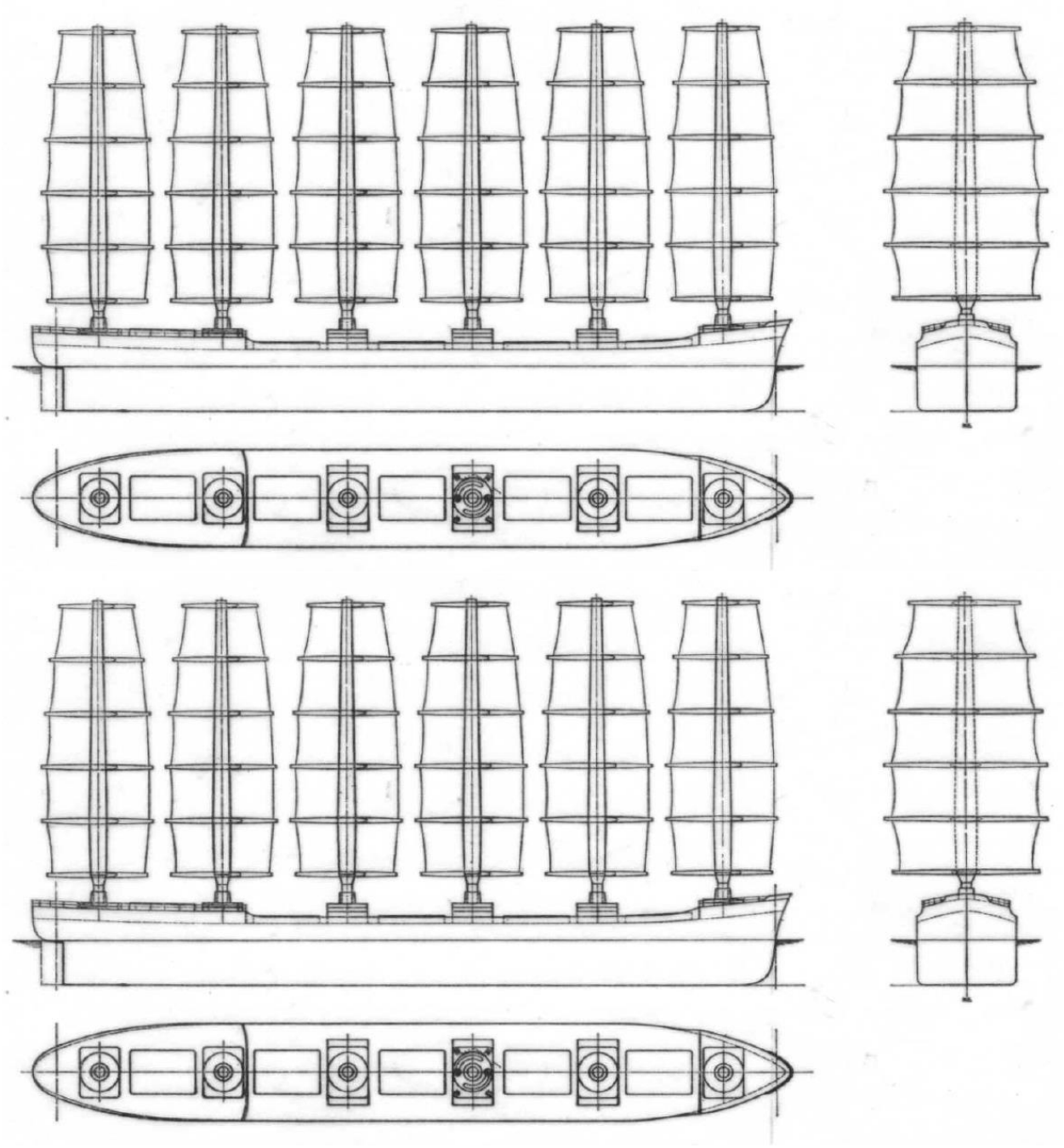

Fig. 2: Wind tunnel model of sailing ship by Prölss, side view: $\delta_S = 45°$; front view: $\delta_S = 90°$

In addition to the model data, the original design data are given below for comparison:

	Main measurements **Hauptabmessungen**		Model Modell	Large version According to Model 1 : 154 Großausführung entsprechend Modell 1 : 154	Original Design IKL Original-Entwurf IKL
LOA	Länge über alles		1,033 m	159,2 m	160,50 m
Lpp	Länge zwischen den Loten		0,980 m	151,0 m	150,80 m
Width	Breite		0,1346 m	20,75 m	21,00 m
Side Height	Seitenhöhe		0,0854 m	13,15 m	13,00 m
Draft	Tiefgang		0,0617 m	9,52 m	9,215 m
Number of Masts	Mastanzahl		6	6	6
Height of Sails	Höhe der Besegelung*)	H =	0,458 m	70,60 m	67,0 m
Projected Sail Area	projizierte Segelfläche	A =	0,4092 m²	9700 m²	9700 m²
Hull lateral Area	Rumpflateralfläche	A_{yR} =	0,0447 m²		
Aspect ratio of the sails	Seitenverhältnis der Besegelung $\Lambda = \frac{H^2}{A}$	=	0,513	0,513	0,494
Minimal setting angle of the masts	minimaler Einstellwinkel der Masten	δ_S =	10°		

*) Größere Masthöhe des Modells im Vergleich zum Originalentwurf ist durch Verstelleinrichtung der Masten bedingt.

*) Greater mast height of the model compared to the original design is due to the mast adjustment device

The hull of the model was made of teak, bulwark and railings were – if present (existing) – made of brass.

The elliptical profile masts are made of light metal (AlMg5)[6]. The cambered yards, made of flat brass 3 x 8 mm, tapered at the ends of the yards, were screwed onto the intended support pin of the mast. They have a curvature (camber) of $f/L_S = 0.120$.

The sailcloth (Dacron 100 mg/m^2) was applied in one piece and stretched over the yards, and held by 0.5 mm thick cover rails. The hyperbolically cut side edges of the section sails have been reinforced with a thin Perlon cord.

The masts are vertical, and are mounted so as to permit continuous rotation and fixing of the masts.

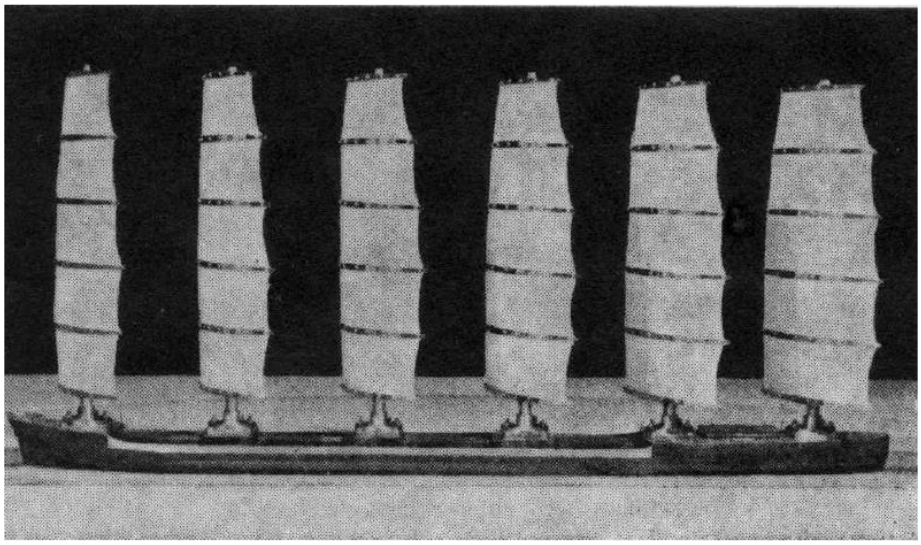

Fig. 3a: Model in wind tunnel, masts positioned parallel, lee view: $\delta_S = 60°$

[6] Magnesium-alloyed aluminum wire (with max. 5% Mg) used as filler metal for welding aluminum alloys (translator's remark)

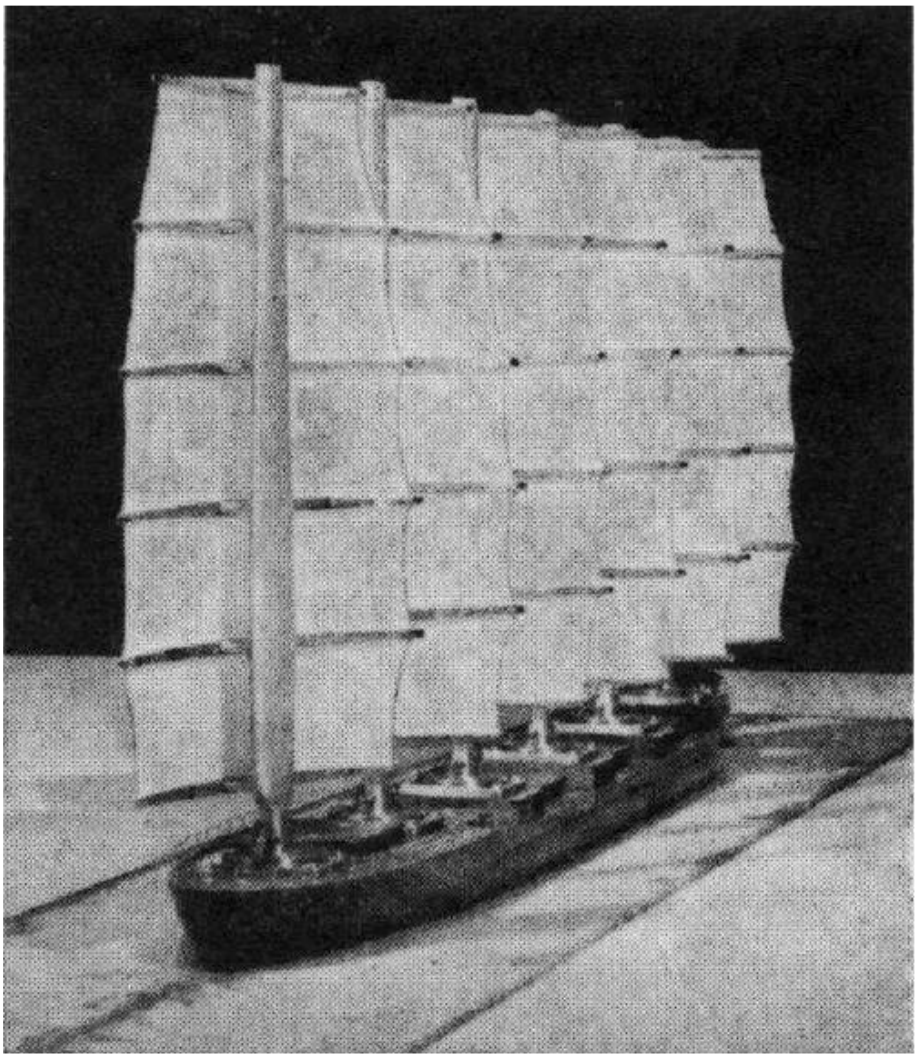

Fig. 3b: Model in wind tunnel, masts staggered, windward view: $\delta_S = 60°/30°$

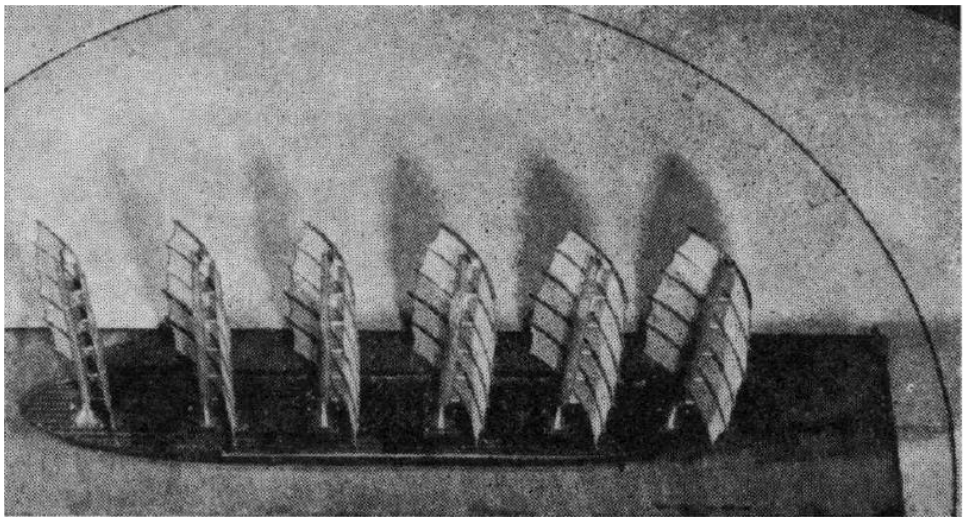

Fig. 3c: Model in wind tunnel, masts parallel, view from above, $\delta_S = 60°$

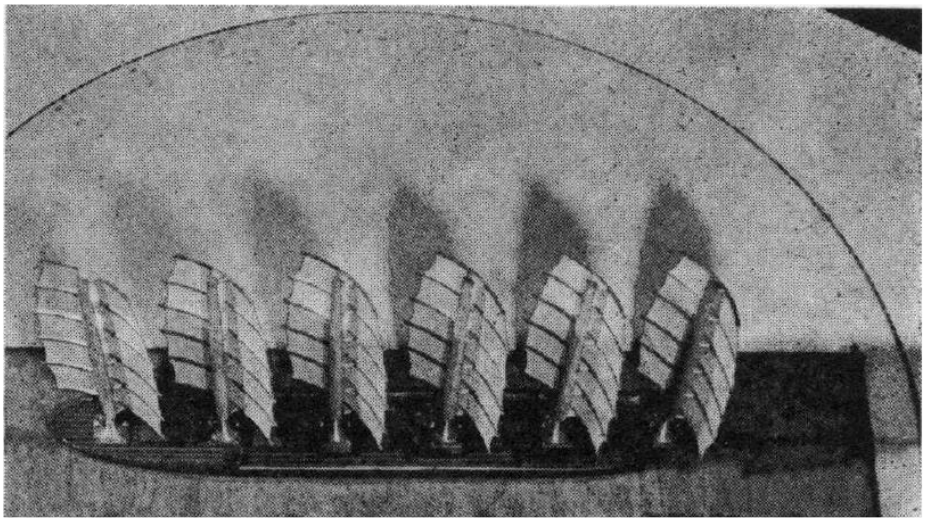

Fig. 3d: Model in wind tunnel, masts staggered, view from above, $\delta_S = 60°/30°$

3. Tests and Test Results
3.1. Tests

The tests were carried out with full sail for the design draft and without trimming and heeling.

The velocity distribution over the tunnel floor is homogeneous except for a starting boundary layer of approx. 25 mm thickness. The antechamber pressure was kept constant during the measurement. The readings were based on the dynamic pressure of the undisturbed flow related to the center of the model.

Beam cross-section:	1.75 m^2
Beam speed:	18.20 m/s
Dynamic pressure[7]:	20.20 kp/m^2
Reynolds number: $R_n = V \cdot L_s/\nu$	$0.240 \cdot 10^6$
Beam obstruction: $\frac{A+A_{yR}}{A_s}$	0.2590

In the present beam obstruction, the influence on the measurement results is low (cf. 3.2).

Execution of the Experiments

The measured force components and moments were dependent on the mast setting angle δ_S (angle between the yards and the ship's longitudinal plane) and the lateral angle of incidence of the wind ε.

For this purpose, the masts were turned in the desired adjusting angle δ_S turned to the ship's longitudinal plane and fixed.

By turning the turntable, the angle of attack was measured from $\varepsilon = \delta_S$ (flow in direction of the square chord of the foremost mast) in 5°- resp. 10°- intervals up to $\varepsilon = \delta_S + 90°$ (flow perpendicular to the yard of the foremost mast).

In addition, tests were made with the model without sails (cf. [1]). Some photos (Fig. 3a to d) taken during the tests show the model in the wind tunnel. In Fig. 3c and d, one can distinguish the two different mast settings ("parallel" and "staggered").

3.2. Measurement Accuracy, Influence of Beam Obstruction and Reynolds number

Detailed information on this can be found in [2]. The measurement accuracy of the measuring amplifiers was in general 0.5% of the maximum measuring range of the respective measured value.

The separately determined **correction values for the forces on the turntable** amounted to an antechamber pressure of $p_V = 20$ kp/m^2 approx. 160 to 320 p (corresponding to 1.4 to 2.8% of the maximum measured value) for the resistance, while they could be neglected for the lateral force.

The reported results were not corrected for the **influence of tunnel obstruction** on dynamic (ram) pressure and oblique flow. According to IfS Report No. 160 [8] one estimates that with the

[7] kp/m^2 = kilopondmetre/m^2 – obsolete unit of torque and energy units no longer used in modern engineering practice. One kilopond equals the force applied to 1 kg due to gravitational acceleration g, thus converting it to 9.80665 N. Hence, 1 kp.m = 9.80655 $kg \cdot m^2/s^2$ = 9.80665 N·m. Here we have $kp/m^2 = kp.m/m^3 = kp/m^2$ = 9.80655 N.m/m^3 = 9.80655 N/m^2 = 9.80655 Pa (contemporary units of pressure). Therefore, the listed values of dynamic pressure in kp/m^2 must be multiplied by a factor of 9.80655 to convert correctly to units of Pa (translator's remark)

blockage present here of 25.9%, the lateral force- and resistance coefficients would have to be increased by a maximum of 5% compared to the measured values.

The Reynolds number influence can be significantly lower compared to the examined four-mast barque (cf. [2]) due to the lack of shrouds and thin spars on the model of the sailing ship by Prölss. Control experiments for a smaller Reynolds number showed no significant change in the coefficients; larger Reynolds numbers could not be investigated because the scales did not allow a greater load.

3.3. Experiments

In Report No. 171 [6], dealing with panel sails in a multi-masted arrangement, it was established that a staggered mast setting in many cases results in a more favorable propulsion effect. For this reason, the experimental program in this work included measuring rigging forces and moments (except for the parallel adjusted masts), also for optimally staggered masts. This staggering involves decreasing the sail angle δ_S in the aft direction (which increases the sail angle of attack to the incoming wind tunnel stream). For technical reasons, the smallest setting angle of $\delta_S = 10°$ was chosen. In the investigation examined here, the adjustment angles are linear from foremost to rearmost. Figure 1 shows angle δ_S as well as other important parameters.

The optimal staggering of the setting angles of the masts looks like this:

δ_S (Mast 1)	δ_S (Mast 6)
15° bis 35°	10°
40° bis 45°	15°
50°	20°
60°	30°
70°	45°
80°	60°
90°	80°

The results for parallel masts setting are shown in Tables 1 to 17 in the Appendix, while those for staggered masts adjustment are included in Tables 18 to 28.

Figures 4 and 5 show the shear force coefficients c_C as function of ε and δ_S for parallel and staggered mast settings. The staggering of the mast adjustment angles causes a lateral force increase of up to 17%, without an increase in sail angle of attack. There is no need for an increase in resistance (drag) coefficient c_D. The coefficients of the yaw moments do not differ much. One must use them in cruising speed calculations, because only a ship with a balanced yaw moment can sail, but they will not be explained in more detail here.

An analysis of the rolling moments showed that the center of area of the sail serves as a good approximation for the sail's center of pressure.

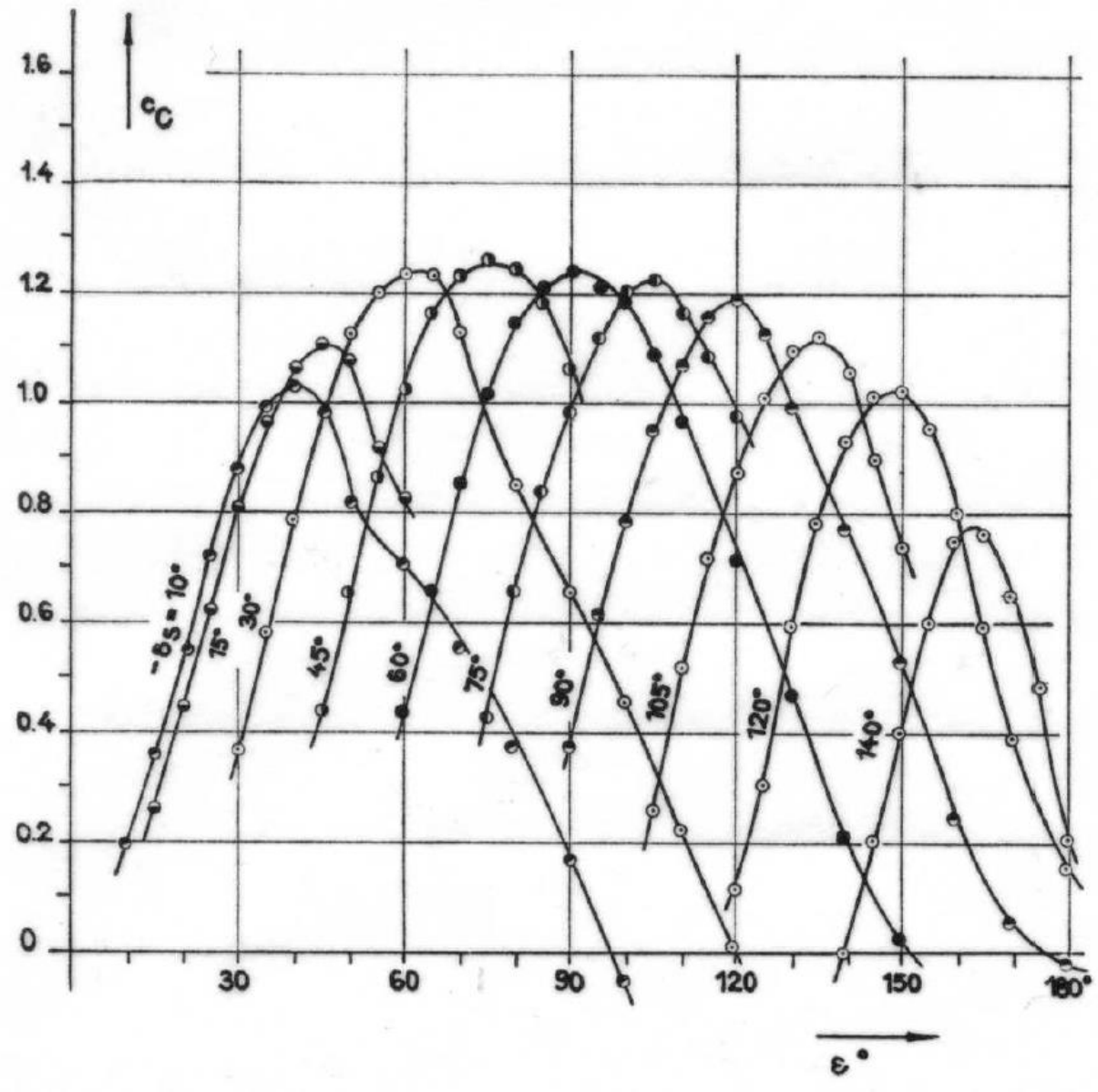

Fig. 4: Sailing ship by Prölss, lateral force coefficient $c_C = f(\varepsilon, \delta_S)$ for parallel masts

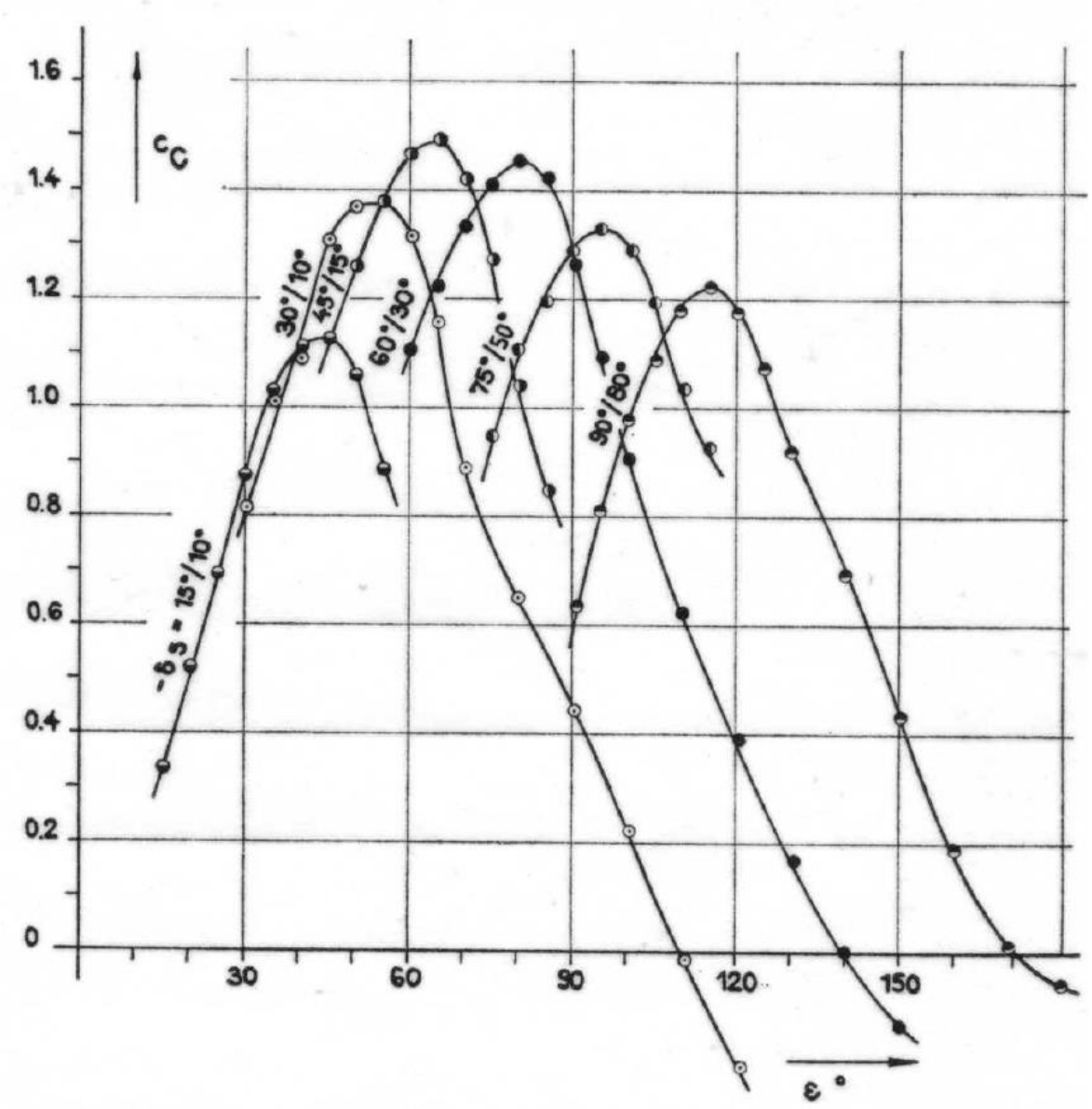

Fig. 5: Sailing ship by Prölss, lateral force coefficient $c_C = f(\varepsilon, \delta_S)$ for staggered masts

3.4. Comparison of the Sail Polars

To compare the rigging and assess the sail characteristics (cruising speed calculations) the sailing theory "sail polars" will be used. This is just a different method of applying the lateral force- and resistance coefficients given in Tables 1 to 28: with the lateral angle of wind incidence ε kept constant, for a certain angle of attack ε_S of the mast, the lateral force (lift) coefficients c_C over the associated resistance (drag) coefficients c_D are plotted and connected by a curve. In a multi-masted sailing ship, these sail polars, consequential from mast interference and hull influence, are strongly depending on ε, which is also what the measurements on the model of the four-masted barque showed (cf. [2]).

In Figures 6 and 7, the sets of the sail polars of the sailing ship by Prölss for parallel and staggered mast adjustment are shown. It turns out that the polars for the small angle of attack of the sail ε_S depend on the lateral angle of incidence of the wind to a far lesser degree than was the case for the four-masted barque.

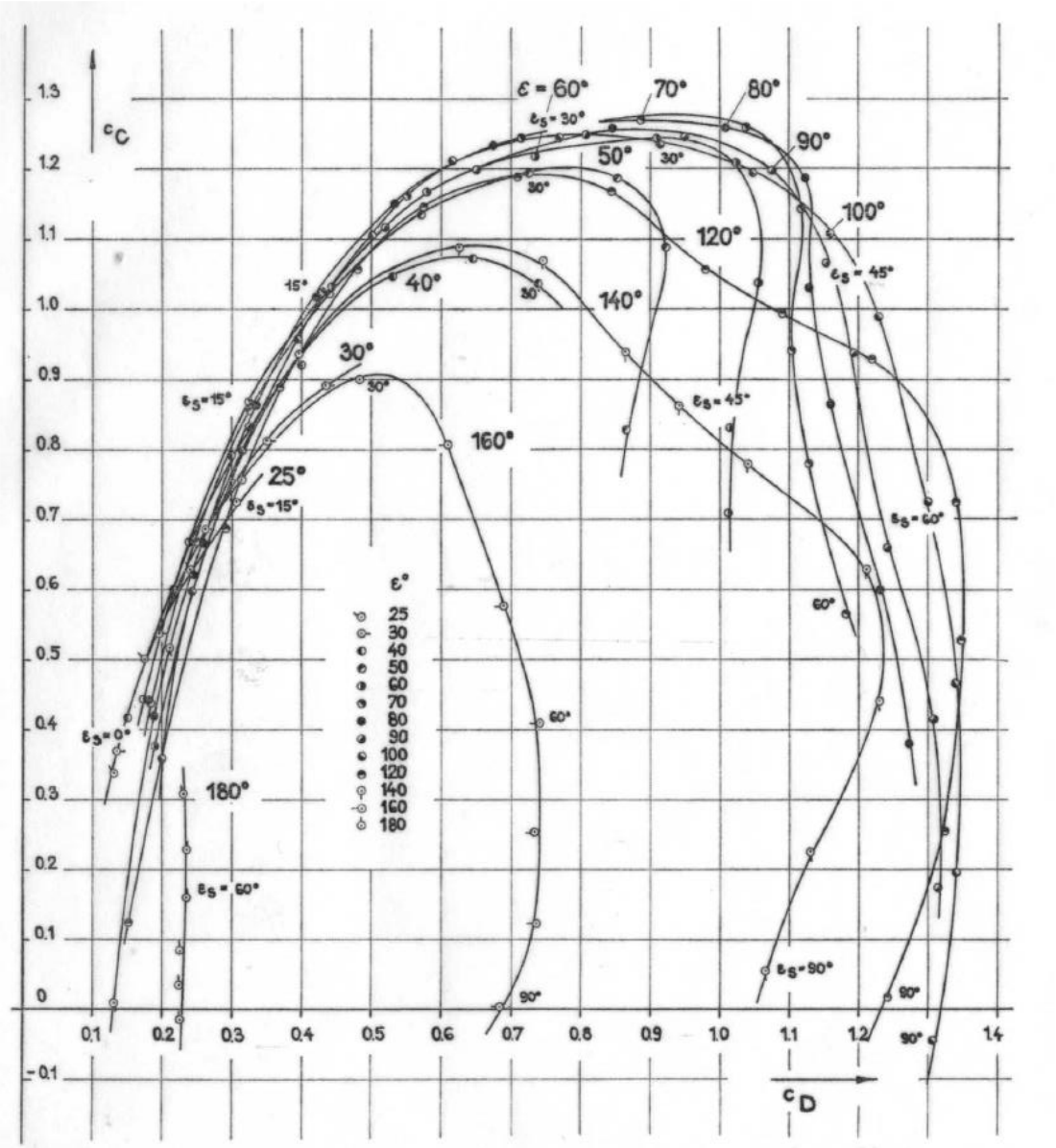

Fig. 6: Sailing ship by Prölss, sail polars $c_C = f(c_D)$ for ε = const., parallel masts, $\Lambda = 0.513$

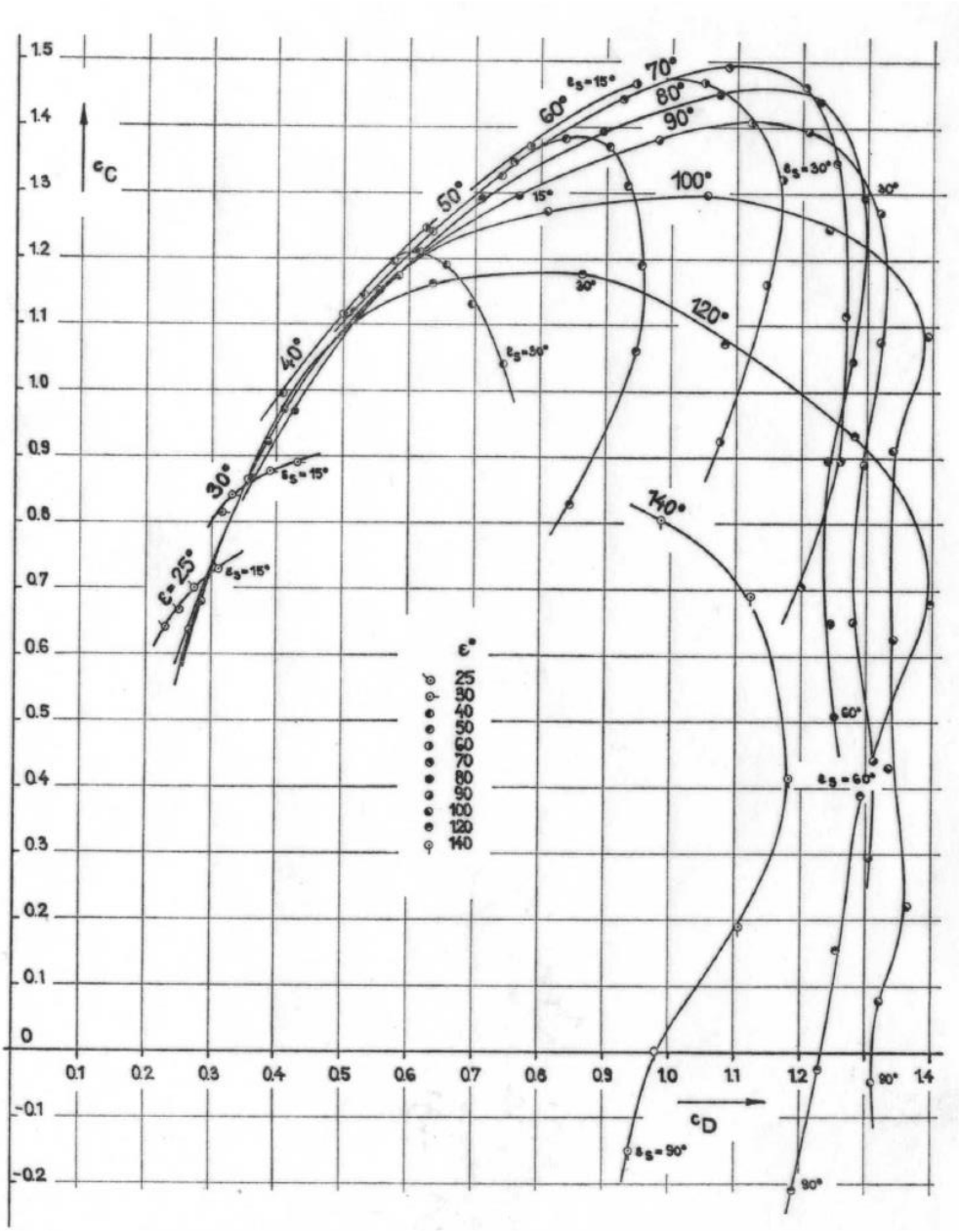

Fig. 7: Sailing ship by Prölss, sail polars $c_C = f(c_D)$ for ε = const., staggered masts, $\Lambda = 0.513$

Figures 8a to 8c compare the sail polars for three ship directions to the wind ε, namely for the courses:

ε = 60° (“close hauled”)
ε = 90° (“beam reach”)
ε = 120° (“broad reach”)

From Fig. 8a (ε = 60°) it can be seen that the larger lift coefficient of the staggered rigging can be achieved throughout a large portion of the plot (avoidance of stronger partial detachment). Figures 8b and 8c show that the benefit of staggering significantly decreases with larger values of ε.

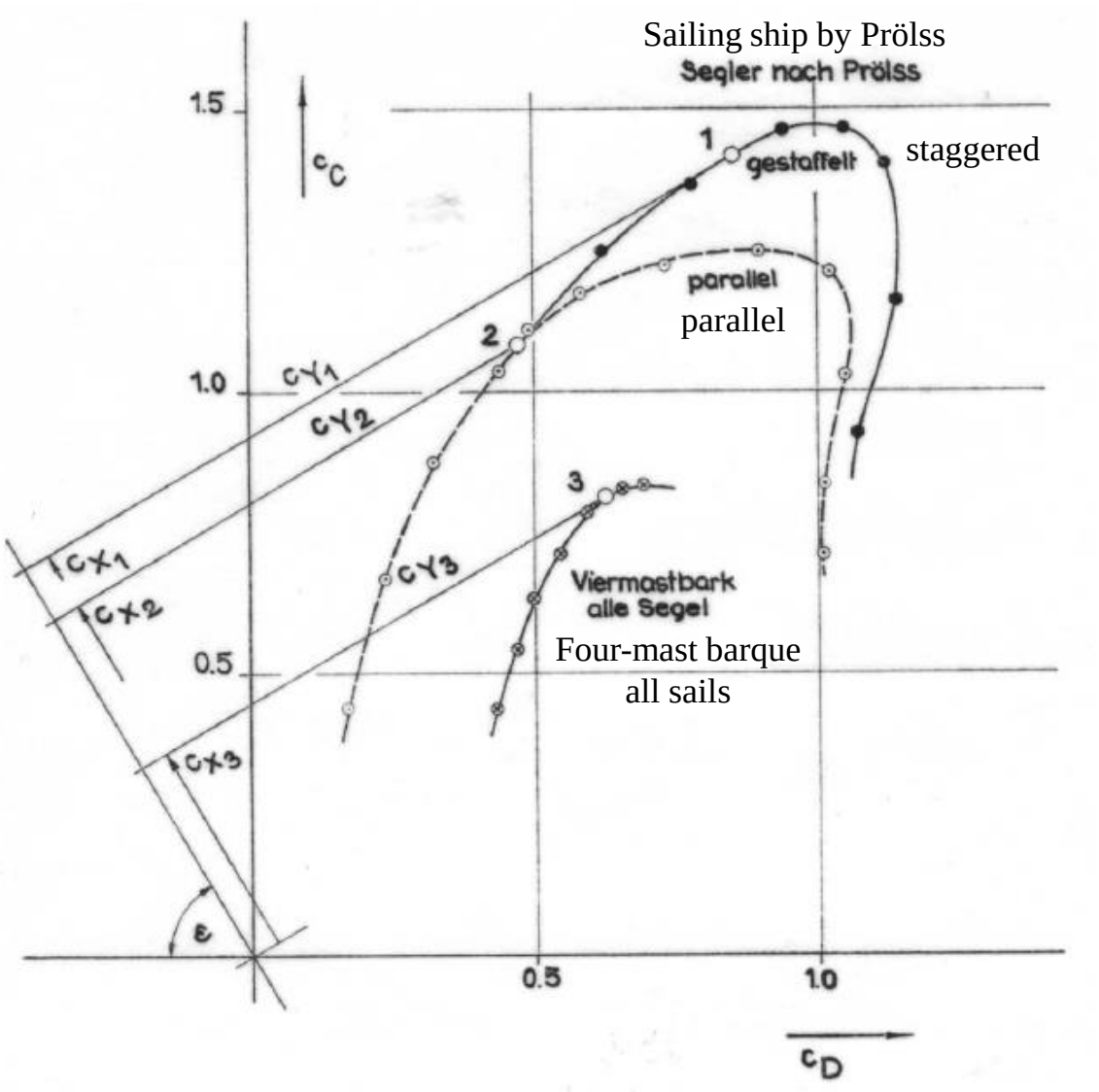

Fig. 8a: Comparison between the sail polars for sailing ship by Prölss and four-masted barque, ε = 6

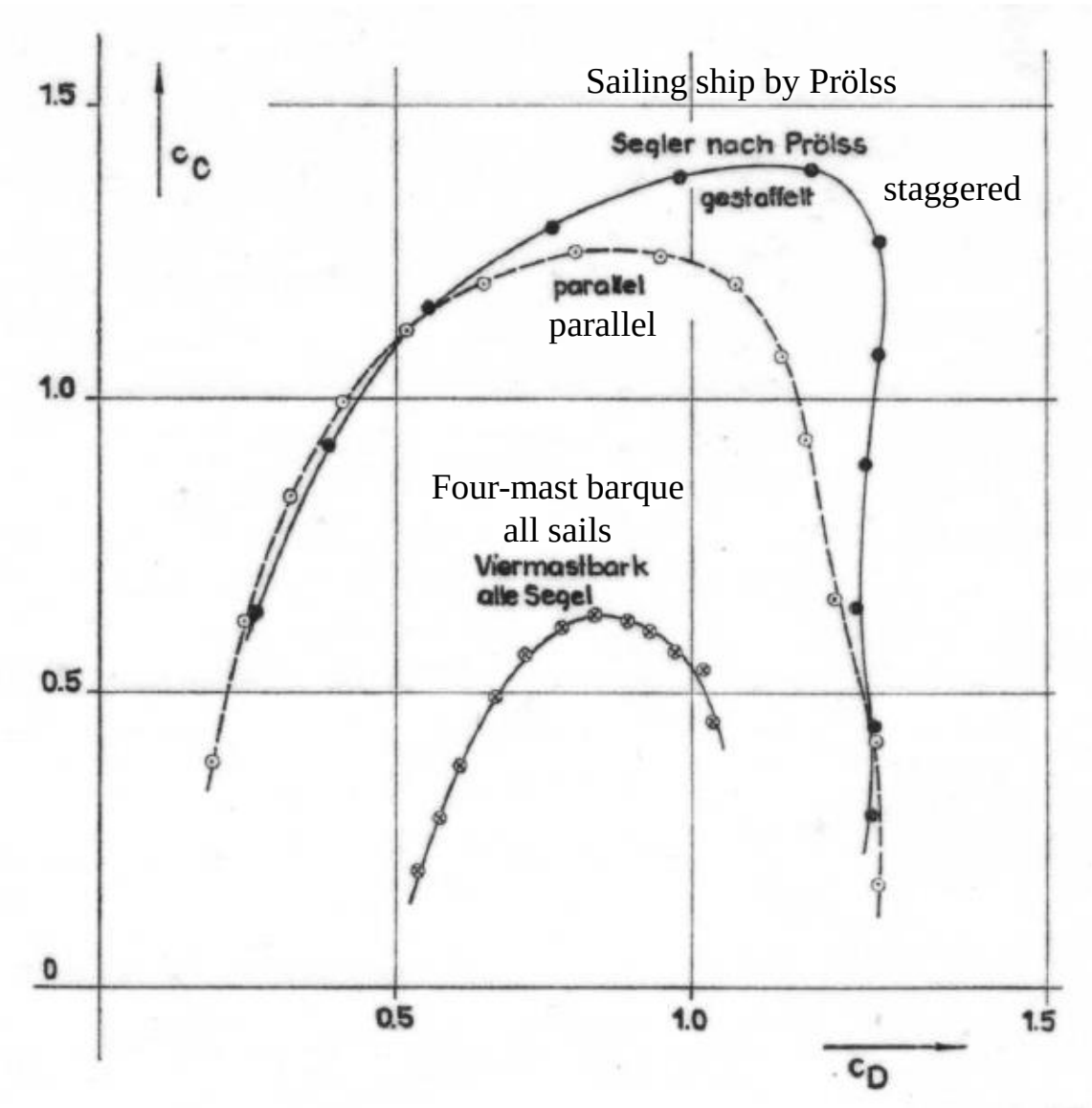

Fig. 8b: Comparison between the sail polars for sailing ship by Prölss and four-masted barque, ε = 90°

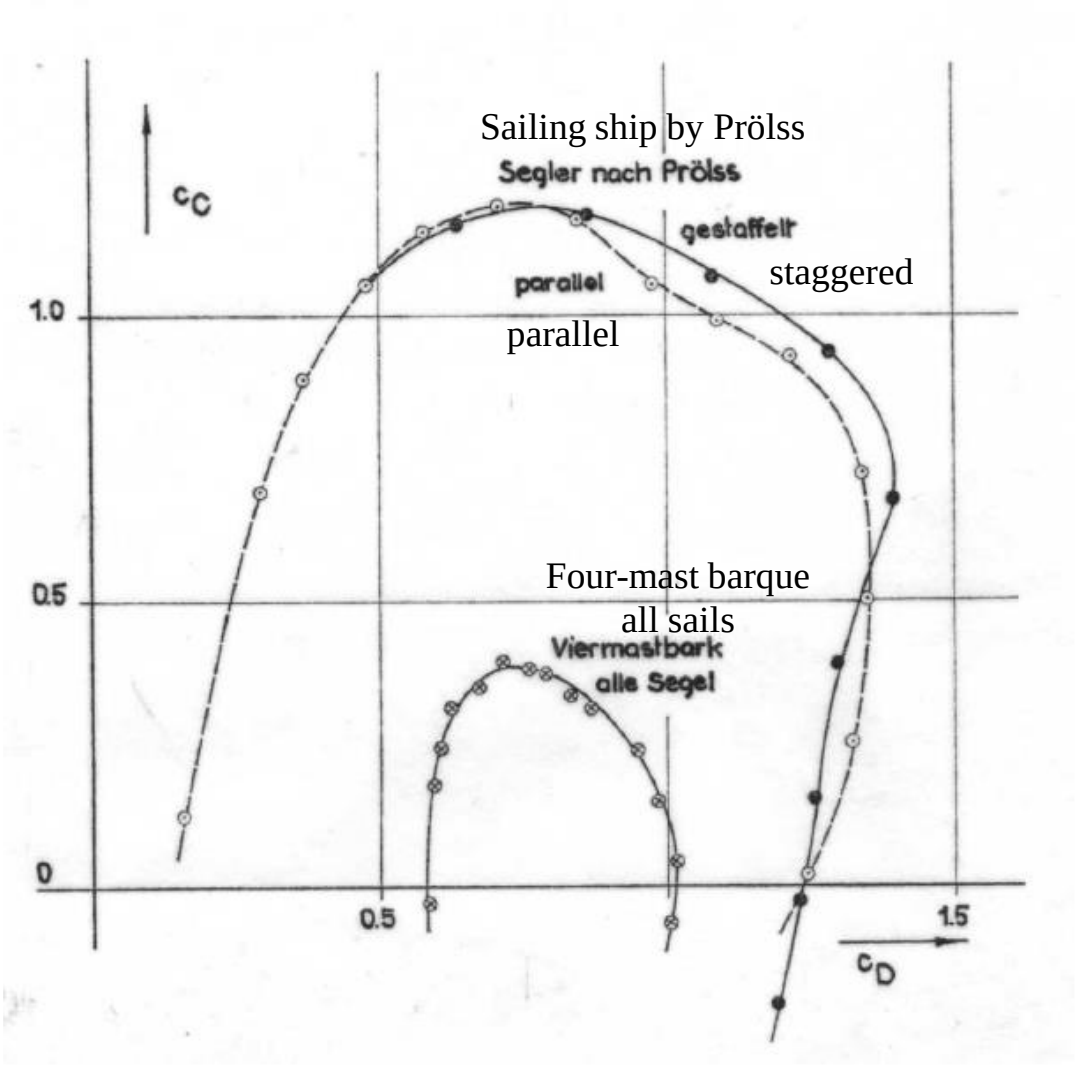

Fig. 8c: Comparison between the sail polars for sailing ship by Prölss and four-masted barque, $\varepsilon = 120°$

Whether the larger lateral force coefficients of the staggered mast setting – especially at higher wind speeds – can also be used depends to a large extent on the stability of the ship. For stability reasons one must often sail with sail positions of the lower polar region (small c_C

values), in which parallel and staggered mast adjustment are not distinguished (see Fig. 8b) or is only achieved for the parallel mast setting (Fig. 8a).

A comparison with the corresponding polars of the four-masted barque (included in Fig. 8a to 8c) is very revealing.

For this purpose, we want the sail force components in the ship's longitudinal direction (c_X) and perpendicular to it (c_Y):

$$c_X = c_C \cdot \sin\varepsilon - c_D \cdot \cos\varepsilon$$
$$c_Y = c_C \cdot \cos\varepsilon + c_D \cdot \sin\varepsilon$$

(see Fig. 1)

In Fig. 8a will be shown how one can obtain these components graphically from the sail polars ("Kurseck", see Croseck [7]): one draws under the angle ε a straight line through the zero point (origin) of the coordinate system. This straight vertical tangent to the sail polar results in the line itself the maximum possible component c_X and the associated perpendicular component c_Y. One can do this component decomposition for any points on the sailing polars through further perpendiculars to the straight line.

One must not consider the acting component in the longitudinal direction of the ship c_X in isolation from its associated component c_Y. The Y-component of the wind force must be equally balanced though a hull force by inclining the hull (drift) in conjunction with a resistance increase of the hull. The comparison of the c_X components, presented in the following table from four-masted barque and the sailing vessel by Prölss for the corresponding angle of incidence of the wind (Fig. 8a to 8c), are therefore carried out for the **same c_Y values**:

Four-masted barque
all sails

	Prölss-Segler Sailing ship by PröIss		Viermastbark alle Segel		$\frac{c_X \text{ (Prölss-S)}}{c_X \text{ (4MBark)}}$ (für gleiches c_Y)	$\frac{c_X \text{ (PröIss-Sailing ship)}}{c_X \text{ (4-M Barque)}}$ (for equal c_Y)
ε	c_X	c_Y	c_X	c_Y		
60°	0,798 max	1,455				
	0,694	0,950	0,390	0,950	1,780	
90°	1,400 max	1,100				
	1,330	0,830	0,630	0,830	2,110	
120°	1,470 max	0,250				
	1,470	0,500	0,720	0,500	2,040	

From the table it can be seen that a measure of the driving force of the rigging in the X-component of the wind force in the longitudinal direction of the ship with the same component Y for the sailing vessel by Prölss in the considered cases is by 78 to 111% above the values of the "conventional" four-masted barque. If one compares it with the sail polar for the four-masted

barque without a staysail (cf. [2]), the comparison is a bit less unfavorable for the four-masted barque.

4. Conclusions

The comparison of sail polars contained in the previous section for a four-masted barque and a sailing vessel by Prölss has shown that the propulsion forces of modern rigging compared to conventional rigging can increase by more than a factor of two. Of course, it is an interesting question to check whether sailing ships equipped with this type of rigging can reach speeds that would be economically justifiable. Such speed calculations have been performed and will be presented in a later work.

5. Summary

Tests were carried out in the IfS wind tunnel on a model of a new sailing ship, and the~~ir~~ results described. The rigging of the new sailing vessel corresponds to a design by W. Prölss. The results are presented in dimensionless form, namely the horizontal force components and the yaw and roll moments, as a function of mast setting and lateral wind angle. The sailing polars were compared to sail polars of a conventional four-masted barque. The comparison shows the propulsion forces of sailing ships is greatly improved by the use of modern designs.

The coworkers of the Institute for Shipbuilding are thanked for supporting this research. Special thanks go to Mr. Böhme for his help with the preparation and implementation of the wind tunnel tests.

6. Symbols

F_R ..... Resulting Force
X ..... Force component in the direction of the towed ship, positive forward
Y ..... Force component perpendicular to the ship's longitudinal plane, positive to starboard
C ..... Force component perpendicular to the flow direction (lateral force), positive in the flow as seen to the left
D ..... Force component in the direction of the flow (resistance), positive in the flow direction
N ..... Moment in the vertical axis, based on $L_{OA}/2$, positive clockwise (yaw moment)
K ..... Moment in the longitudinal axis in the waterline level, positive clockwise (rolling moment)
c_X, c_Y, c_C, c_D Dimensionless coefficients of the forces, based on the pressure of the flow velocity
c_N ..... Dimensionless coefficient of the moments in the vertical axis, based on dynamic pressure of the flow velocity, sail area projection and overall length L_{OA}
c_K ..... Dimensionless coefficient of the moments in the longitudinal axis (rolling moments), based on dynamic pressure of the flow velocity, sail area projection and sail height H
V ..... Relative flow velocity
ϱ ..... Air density under test conditions
$q = \varrho \cdot V^2/2$ Dynamic pressure of flow velocity
q_V ..... Pre-chamber pressure of the wind tunnel
ν ..... Kinematic viscosity of air under test conditions
L_S ..... Chord length of the longest yard of the single mast
L_{OA} ..... Length overall
$R_n = V \cdot L_S/\nu$ Sail Re number
A ..... Sail projection area
A_{yR} ..... Area of the hull side
A_S ..... Beam cross-section of the wind tunnel
H ..... Sail height
$\Lambda = H^2/A$. Sail projected area
e ..... Pressure point location, i.e., distance of the intersection of the resultant with the ship's longitudinal plane form the front
e/L_{OA} ..... Relative pressure point location
ε_S ..... Relative angle of attack of the single mast, based on the yard chord, with staggered mast adjustment angle of attack of the foremost mast
ε ..... Relative angle of attack of the ship, based on the positive x-direction (Direction of the ship's longitudinal plane form the front)
δ_S ..... Setting angle of the single mast, angle between yards and ship's longitudinal plane

7. Literature

[1] B. Wagner: Windkanalversuche für einen sechsmastigen Segler nach Prölss. IfS-Bericht Nr. 173, Januar 1967.

[2] B. Wagner: Windkanalversuche mit dem Takelagemodell einer Viermastbark. IfS-Bericht Nr. 172, Oktober 1966. „Schiff und Hafen", Heft 1/1967, S. 13.

[3] B. Wagner: Praktische Durchführung der Berechnung der Fahrtgeschwindigkeit von Segelschiffen. IfS-Bericht Nr. 112, Juni 1962.

[4] B. Wagner: Windkanalversuche mit gewölbten Plattensegeln an einem rahgetakelten elliptischen Mast neuer freitragender Konstruktion. IfS-Bericht Nr. 122, Juni 1964.

[5] B. Wagner: Windkanalversuche für einen rahgetakelten Mast mit einer gewölbten Platte bei verschiedenen Leesegel-Einstellungen. IfS-Bericht Nr. 123, Juni 1964.

[6] B. Wagner: Windkanalversuche mit gewölbten Plattensegeln mit Einzelmasten sowie mit Plattensegeln bei Mehrmastanordnung. IfS-Bericht Nr. 171, Oktober 1966.

[7] H. Croseck: „Beiträge zur Theorie des Segelns". Verlag von Julius Springer, Berlin 1925.

[8] B. Wagner: Windkanalversuche mit Schiffssilhouetten und Rechteckplatten zur Prüfung des Versperrungseinflusses in einem Rechteckstrahl. IfS-Bericht Nr. 160 (in Vorbereitung).

Attachment: Wind Tunnel Results (next page)

Model of sailing ship by Prölss **Modell Segler nach Prölss**
Masts parallel **Masten parallel eingestellt** $A = 0{,}4092\ m^2$; $L_{OA} = 1{,}033\ m$

Tab. 1: — $\delta_S = 10°$; $R_n = 0{,}242 \cdot 10^6$

ε_S	c_C	c_D	c_N	c_K
0	0.209	0.098	0.0326	0.124
5	0.368	0.140	0.0590	—
10	0.555	0.210	0.0922	0.309
15	0.729	0.307	0.1261	0.446
20	0.883	0.435	0.1577	0.525
25	1.001	0.592	0.1758	0.578
30	1.039	0.741	0.1912	0.622
35	0.989	0.831	0.1501	—
40	0.828	0.864	0.0891	0.604
50	0.710	1.013	0.0661	—
60	0.565	1.184	0.0377	0.617
70	0.379	1.273	0.0274	—
80	0.174	1.316	0.0141	—
90	—0.043	1.311	0.0004	0.627

Tab. 2: — $\delta_S = 15°$; $R_n = 0{,}243 \cdot 10^6$

ε_S	c_C	c_D	c_N
0	0.267	0.114	0.0420
5	0.451	0.162	0.0684
10	0.630	0.237	0.0960
15	0.815	0.348	0.1291
20	0.976	0.491	0.1551
25	1.076	0.645	0.1723
30	1.113	0.805	0.1834
35	1.088	0.925	0.1518
40	0.927	0.974	0.0958
45	0.832	1.016	0.0648

Tab. 3: — $\delta_S = 20°$; $R_n = 0{,}242 \cdot 10^6$

ε_S	c_C	c_D	c_N
0	0.307	0.120	0.0465
5	0.503	0.176	0.0690
10	0.680	0.261	0.0980
15	0.883	0.377	0.1193
20	1.045	0.532	0.1506
25	1.151	0.697	0.1670
30	1.189	0.854	0.1697
35	1.176	0.992	0.1515
40	1.039	1.054	0.0961
50	0.779	1.128	0.0416
60	0.599	1.230	0.0222
70	0.416	1.311	0.0189
80	0.196	1.342	0.0143
90	—0.023	1.292	0.0051

Tab. 4: — $\delta_S = 30°$; $R_n = 0{,}242 \cdot 10^6$

ε_S	c_C	c_D	c_N	c_K
0	0.373	0.134	0.0488	0.185
5	0.590	0.200	0.0683	—
10	0.797	0.299	0.0877	0.406
15	0.982	0.425	0.1086	0.501
20	1.138	0.573	0.1174	0.565
25	1.210	0.741	0.1268	0.620
30	1.246	0.901	0.1309	0.657
35	1.246	1.044	0.1229	0.675
40	1.144	1.117	0.0878	0.670
50	0.865	1.160	0.0366	—
60	0.661	1.242	0.0135	0.615
70	0.463	1.339	0.0196	—
80	0.231	1.317	0.0234	—
90	0.018	1.242	0.0135	0.541

Tab. 5: — $\delta_S = 40°$; $R_n = 0{,}242 \cdot 10^6$

ε_S	c_C	c_D	c_N
0	0.422	0.152	0.0414
5	0.655	0.224	0.0527
10	0.859	0.324	0.0668
15	1.038	0.448	0.0745
20	1.170	0.581	0.0849
25	1.246	0.731	0.0932
30	1.270	0.890	0.0907
35	1.258	1.029	0.0941
40	1.186	1.124	0.0654
45	1.063	1.135	0.0386
50	0.933	1.196	0.0289
60	0.723	1.298	0.0184
70	0.496	1.354	0.0144
80	0.255	1.323	0.0190
90	0.044	1.206	0.0312

Tab. 6: — $\delta_S = 45°$; $R_n = 0{,}241 \cdot 10^6$

ε_S	c_C	c_D	c_N	c_K
0	0.448	0.155	0.0322	0.185
5	0.667	0.233	0.0435	—
10	0.871	0.327	0.0500	0.377
15	1.036	0.443	0.0590	0.446
20	1.176	0.573	0.0680	0.501
25	1.246	0.713	0.0728	0.540
30	1.270	0.868	0.0697	0.557
35	1.258	1.010	0.0745	—
40	1.192	1.100	0.0643	0.562
45	1.071	1.154	0.0334	—

Tab. 7: — $\delta_S = 50°$; $R_n = 0{,}240 \cdot 10^6$

ε_S	c_C	c_D	c_N
0	0.440	0.186	0.0100
5	0.667	0.235	0.0356
10	0.871	0.325	0.0394
15	1.051	0.433	0.0479
20	1.164	0.553	0.0555
25	1.222	0.700	0.0665
30	1.258	0.844	0.0554
35	1.258	0.979	0.0570
40	1.198	1.074	0.0415
45	1.119	1.150	0.0263
50	0.989	1.230	0.0222
60	0.760	1.336	0.0099
70	0.503	1.348	0.0188
80	0.255	1.255	0.0317
90	0.054	1.063	0.0397

Tab. 8: — $\delta_S = 60°$; $R_n = 0{,}242 \cdot 10^6$

ε_S	c_C	c_D	c_N	c_K
0	0.443	0.172	0.0191	0.174
5	0.667	0.244	0.0184	—
10	0.863	0.330	0.0218	0.312
15	1.026	0.423	0.0284	0.346
20	1.151	0.532	0.0359	0.375
25	1.216	0.658	0.0423	0.393
30	1.252	0.801	0.0440	0.398
35	1.222	0.929	0.0412	—
40	1.195	1.048	0.0334	0.414
45	1.101	1.156	0.0220	—
50	0.976	1.236	0.0178	—
60	0.723	1.342	0.0055	0.409
70	0.472	1.292	0.0139	—
80	0.226	1.128	0.0332	—
90	0.034	1.053	—0.0543	0.219

Tab. 9: — $\delta_S = 70°$; $R_n = 0{,}241 \cdot 10^6$

ε_S	c_C	c_D	c_N
0	0.434	0.183	0.0064
5	0.673	0.249	0.0044
10	0.859	0.327	0.0095
15	1.014	0.414	0.0177
20	1.119	0.520	0.0217
25	1.198	0.635	0.0307
30	1.246	0.769	0.0371
35	1.188	0.892	0.0197
40	1.126	1.010	0.0172
50	0.927	1.218	0.0133
60	0.704	1.336	0.0099
70	0.442	1.230	0.0222
80	0.181	0.987	0.0209
90	0.006	0.685	0.0130

Tab. 10: — $\delta_S = 75°$; $R_n = 0{,}241 \cdot 10^6$

ε_S	c_C	c_D	c_N	c_K
0	0.434	0.187	—0.0006	0.118
5	0.667	0.251	—0.0009	—
10	0.847	0.327	0.0024	0.167
15	0.995	0.410	0.0097	0.173
20	1.125	0.516	0.0190	0.173
25	1.213	0.616	0.0226	0.171
30	1.234	0.759	0.0300	0.167
35	1.176	0.868	0.0195	—
40	1.095	0.997	0.0188	0.170
45	0.995	1.089	0.0135	—

Tab. 11: — $\delta_S = 80°$; $R_n = 0{,}241 \cdot 10^6$

ε_S	c_C	c_D	c_N
0	0.422	0.189	—0.0036
90	0.000	0.302	—0.0079
10	0.835	0.325	0.0006
15	0.976	0.402	0.0070
20	1.107	0.501	0.0167
25	1.182	0.610	0.0177
30	1.192	0.742	0.0259
35	1.157	0.861	0.0247
40	1.057	0.977	0.0125
50	0.871	1.151	0.0127
60	0.630	1.212	0.0176
70	0.354	1.004	0.0224
80	0.126	0.734	0.0139
90	0.000	0.302	—0.0079

Tab. 12: — $\delta_S = 90°$; $R_n = 0{,}243 \cdot 10^6$

ε_S	c_C	c_D	c_N
0	0.381	0.190	—0.0116
5	0.624	0.253	—0.0132
10	0.797	0.315	0.0083
15	0.958	0.400	0.0026
20	1.077	0.482	0.0117
25	1.170	0.592	0.0188
30	1.192	0.708	0.0225
35	1.138	0.823	0.0147
40	1.002	0.919	0.0173
50	0.780	1.039	0.0170
60	0.541	0.996	0.0237
70	0.256	0.735	0.0148
80	0.062	0.329	—0.0007
90	—0.011	0.223	0.0002

Tab. 13: — $\delta_S = 100°$; $R_n = 0{,}243 \cdot 10^6$

ε_S	c_C	c_D	c_N
0	0.358	0.197	—0.0190
5	0.596	0.252	—0.0159
10	0.785	0.319	—0.0074
15	0.927	0.397	0.0035
20	1.057	0.480	0.0170
25	1.129	0.587	0.0135
30	1.151	0.693	0.0074
35	1.082	0.800	0.0083
40	0.939	0.864	0.0124
50	0.667	0.893	0.0201
60	0.408	0.742	0.0166
70	0.137	0.373	0.0085
80	0.037	0.224	0.0152

Tab. 14: — $\delta_S = 105°$; $R_n = 0{,}243 \cdot 10^6$

ε_S	c_C	c_D	c_N
0	0.268	0.178	—0.0218
5	0.531	0.230	—0.0178
10	0.723	0.295	—0.0089
15	0.889	0.367	0.0041
20	1.020	0.451	0.0167
25	1.107	0.544	0.0144
30	1.132	0.648	0.0109
35	1.069	0.745	0.0083
40	0.909	0.792	0.0153
45	0.754	0.809	0.0234

Tab. 15: — $\delta_S = 110°$; $R_n = 0{,}241 \cdot 10^6$

ε_S	c_C	c_D	c_N
0	0.237	0.172	—0.0245
5	0.490	0.225	—0.0183
10	0.692	0.291	—0.0067
15	0.865	0.356	0.0049
20	1.002	0.440	0.0193
25	1.089	0.535	0.0210
30	1.089	0.625	0.0098
35	1.038	0.717	0.0049
40	0.877	0.748	0.0074
50	0.534	0.665	0.0111
60	0.229	0.397	0.0087
70	0.087	0.223	0.0249

Tab. 16: — $\delta_S = 120°$; $R_n = 0{,}241 \cdot 10^6$

ε_S	c_C	c_D	c_N
0	0.123	0.152	—0.0313
5	0.363	0.180	—0.0209
10	0.605	0.245	—0.0054
15	0.791	0.316	0.0072
20	0.939	0.393	0.0197
25	1.026	0.483	0.0192
30	1.032	0.563	0.0018
35	0.964	0.614	—0.0180
40	0.809	0.608	—0.0216
45	0.605	0.555	—0.0278
50	0.400	0.423	—0.0087
60	0.161	0.236	0.0259

Tab. 17: — $\delta_S = 140°$; $R_n = 0{,}242 \cdot 10^6$

ε_S	c_C	c_D	c_N
0	0.010	0.129	—0.0359
5	0.211	0.136	—0.0134
10	0.416	0.172	0.0112
15	0.612	0.237	0.0360
20	0.760	0.314	0.0517
25	0.772	0.357	0.0168
30	0.661	0.367	0.0036
35	0.496	0.305	—0.0004
40	0.311	0.230	0.0104

Model of sailing ship by Prölss **Modell Segler nach Prölss**
Masts staggered **Masten gestaffelt eingestellt** A = 0,4092 m²; L_{OA} = 1,093 m

Tab. 18: $-\delta_S = 15°/10°$; $R_n = 0{,}240 \cdot 10^6$

ε_S	c_C	c_D	c_N
0	0.333	0.130	0.0324
5	0.521	0.188	0.0625
10	0.698	0.273	0.0945
15	0.877	0.391	0.1277
20	1.022	0.540	0.1551
25	1.113	0.694	0.1732
30	1.123	0.838	0.1000
35	1.057	0.944	0.1462
40	0.883	0.972	0.0795

Tab. 19: $-\delta_S = 20°/10°$; $R_n = 0{,}240 \cdot 10^6$

ε_S	c_C	c_D	c_N
0	0.484	0.171	0.0293
5	0.667	0.248	0.0542
10	0.865	0.356	0.0838
15	1.045	0.495	0.1145
20	1.188	0.654	0.1472
25	1.210	0.814	0.1680
30	1.198	0.932	0.1604
35	1.119	1.057	0.1410
40	0.927	1.074	0.0737
50	0.704	1.148	0.0373
60	0.509	1.255	0.0136
70	0.293	1.303	0.0140
80	0.079	1.322	0.0001
90	−0.134	1.268	−0.0225

Tab. 20: $-\delta_S = 30°/10°$; $R_n = 0{,}241 \cdot 10^6$

ε_S	c_C	c_D	c_N	c_K
0	0.813	0.313	0.0030	0.433
5	1.008	0.439	0.0298	—
10	1.194	0.573	0.0583	0.620
15	1.307	0.728	0.0875	0.701
20	1.367	0.903	0.1062	0.777
25	1.379	1.047	0.1321	0.805
30	1.319	1.169	0.1302	0.820
35	1.157	1.231	0.0967	0.775
40	0.896	1.208	0.0312	0.713
50	0.648	1.242	0.0223	—
60	0.442	1.311	0.0097	0.671
70	0.219	1.361	−0.0084	—
80	−0.013	1.279	−0.0043	—
90	−0.211	1.188	−0.0002	0.586

Tab. 21: $-\delta_S = 40°/15°$; $R_n = 0{,}241 \cdot 10^6$

ε_S	c_C	c_D	c_N
0	0.996	0.416	−0.0033
5	1.182	0.544	−0.0014
10	1.307	0.702	0.0180
15	1.391	0.847	0.0391
20	1.464	1.000	0.0656
25	1.428	1.127	0.0746
30	1.343	1.230	0.0830
35	1.169	1.307	0.0506
40	0.896	1.238	0.0095
50	0.648	1.279	0.0045
60	0.428	1.336	0.0011
70	0.191	1.299	0.0003
80	−0.024	1.230	0.0045
90	−0.188	1.063	0.0119

Tab. 22: $-\delta_S = 45°/15°$; $R_n = 0{,}244 \cdot 10^6$

ε_S	c_C	c_D	c_N	c_K
0	1.125	0.509	−0.0414	0.574
5	1.258	0.648	−0.0239	—
10	1.379	0.794	−0.0037	0.715
15	1.464	0.945	0.0162	0.766
20	1.494	1.097	0.0400	0.800
25	1.422	1.220	0.0613	0.808
30	1.283	1.296	0.0310	0.786
35	1.045	1.275	0.0102	0.727
40	0.853	1.262	0.0013	0.680

Tab. 23: $-\delta_S = 50°/20°$; $R_n = 0{,}243 \cdot 10^6$

ε_S	c_C	c_D	c_N
0	1.119	0.514	−0.0533
5	1.240	0.639	−0.0390
10	1.367	0.785	−0.0236
15	1.452	0.935	−0.0068
20	1.488	1.085	0.0117
25	1.452	1.230	0.0270
30	1.284	1.296	0.0241
35	1.083	1.307	−0.0129
40	0.889	1.294	0.0047
50	0.624	1.342	−0.0033
60	0.379	1.336	0.0011
70	0.155	1.255	0.0136
80	−0.030	1.118	0.0082
90	−0.151	0.939	0.0293

Tab. 24: $-\delta_S = 60°/30°$; $R_n = 0{,}241 \cdot 10^6$

ε_S	c_C	c_D	c_N	c_K
0	1.113	0.499	−0.0858	0.504
5	1.222	0.628	−0.0558	—
10	1.343	0.760	−0.0414	0.585
15	1.415	0.900	−0.0363	0.625
20	1.452	1.070	−0.0237	0.637
25	1.428	1.224	−0.0127	0.662
30	1.270	1.320	−0.0127	0.646
35	1.089	1.319	−0.0392	—
40	0.909	1.337	−0.0254	0.583
50	0.624	1.330	−0.0122	—
60	0.387	1.292	0.0060	0.509
70	0.169	1.149	0.0171	—
80	0.000	0.981	0.0253	—
90	−0.132	0.784	0.0139	—

Tab. 25: $-\delta_S = 70°/45°$; $R_n = 0{,}242 \cdot 10^6$

ε_S	c_C	c_D	c_N
0	0.970	0.422	−0.0539
5	1.131	0.524	−0.0479
10	1.234	0.647	−0.0407
15	1.307	0.784	−0.0337
20	1.355	0.935	−0.0337
25	1.367	1.093	−0.0332
30	1.346	1.241	−0.0364
35	1.089	1.319	−0.0480
40	0.982	1.399	−0.0606
50	0.680	1.397	−0.0346
60	0.416	1.286	−0.0003
70	0.188	1.106	0.0079
80	0.000	0.909	0.0016
90	−0.116	0.610	−0.0141

Tab. 26: $-\delta_S = 75°/50°$; $R_n = 0{,}240 \cdot 10^6$

ε_S	c_C	c_D	c_N	c_K
0	0.952	0.419	−0.0576	0.347
5	1.113	0.521	−0.0471	—
10	1.198	0.633	−0.0452	0.382
15	1.294	0.766	−0.0418	0.397
20	1.331	0.915	−0.0427	0.407
25	1.294	1.053	−0.0398	0.428
30	1.198	1.200	−0.0473	0.431
35	1.038	1.276	−0.0625	0.438
40	0.927	1.367	−0.0657	0.430

Tab. 27: $-\delta_S = 80°/60°$; $R_n = 0{,}243 \cdot 10^6$

ε_S	c_C	c_D	c_N
0	0.865	0.359	−0.0405
5	1.020	0.448	−0.0353
10	1.151	0.553	−0.0282
15	1.234	0.670	−0.0277
20	1.270	0.801	−0.0349
25	1.258	0.955	−0.0362
30	1.213	1.093	−0.0324
35	1.045	1.187	−0.0377
40	0.933	1.282	−0.0395
50	0.692	1.354	−0.0402
60	0.416	1.181	−0.0056
70	0.175	0.957	−0.0119
80	0.012	0.645	0.0164
90	−0.075	0.264	−0.0365

Tab. 28: $-\delta_S = 90°/80°$; $R_n = 0{,}243 \cdot 10^6$

ε_S	c_C	c_D	c_N
0	0.636	0.264	−0.0255
5	0.815	0.335	−0.0169
10	0.970	0.413	−0.0101
15	1.089	0.509	−0.0017
20	1.182	0.612	−0.0039
25	1.221	0.739	−0.0072
30	1.176	0.862	−0.0070
35	1.076	0.974	−0.0131
40	0.927	1.042	−0.0081
50	0.692	1.121	−0.0087
60	0.434	0.982	0.0068
70	0.188	0.699	0.0043
80	0.012	0.389	−0.0150
90	−0.053	0.227	−0.0174